Int. J. Plant Sci. 168(8):1113–1126. 2007.

1058-5893/2007/16808-0001$15.00 DOI: 10.1086/520724

WATER TRANSPORT IN VESSELLESS ANGIOSPERMS: CONDUCTING EFFICIENCY AND CAVITATION SAFETY

U. G. Hacke,* J. S. Sperry,[1],† T. S. Feild,‡ Y. Sano,§ E. H. Sikkema,† and J. Pittermann‖

*Department of Renewable Resources, University of Alberta, Edmonton T6G 2H1, Canada; †Department of Biology, University of Utah, 257S 1400E, Salt Lake City, Utah 84112, U.S.A.; ‡Department of Ecology and Evolutionary Biology, University of Tennessee, Knoxville, Tennessee 37996, U.S.A.; §Laboratory of Woody Plant Biology, Graduate School of Agriculture, Hokkaido University, Sapporo 060-8589, Japan; and ‖Department of Integrative Biology, University of California, Berkeley, California 94720, U.S.A.

Two structure-function hypotheses were tested for vesselless angiosperm wood. First, vesselless angiosperm wood should have much higher flow resistance than conifer wood because angiosperm tracheids lack low-resistance torus-margo pits. Second, vesselless wood ought to be exceptionally safe from cavitation if the small cumulative area of pits between tracheids confers safety (the pit area hypothesis). Data were obtained from branch wood of 19 vesselless angiosperms: *Amborella trichopoda*, *Trochodendron aralioides*, *Tetracentron sinense*, and 16 Winteraceae from *Tasmannia*, *Zygogynum*, *Bubbia*, *Pseudowintera*, and *Drimys*. Contrary to the first hypothesis, vesselless and conifer species with narrow tracheids (below ca. 18 μm) had similar area-specific resistivities. The reason was that vesselless angiosperms had an intertracheid pit resistance (mean 16 ± 2 MPa s m^{-1}) that was nearly as low as that of conifers (6 ± 1 MPa s m^{-1}) and much lower than that of eudicot intervessel pits (336 ± 81 MPa s m^{-1}). Low pit resistance was associated with greater pit membrane porosity inferred from scanning electron microscopy observations and silicone penetration and may represent incipient pit membrane loss. Pit resistance was often greater in wider angiosperm tracheids and obscured any drop in wood resistivity with tracheid width. In support of the second hypothesis, vesselless woods averaged a cavitation pressure of -3.4 ± 0.3 MPa, which is low for their wet habitats. In agreement with the pit area hypothesis, resistance to cavitation increased with decreasing total pit area between conduits. However, vesselless angiosperms were more vulnerable for a given pit area than eudicots, consistent with their more permeable pit membranes. Small total pit area between conduits may allow angiosperm tracheids to have more porous membranes for conducting efficiency without creating a cavitation problem.

Keywords: basal angiosperm physiology, cavitation, ecological wood anatomy, vesselless angiosperms, xylem and vessel evolution.

Introduction

The ancestral angiosperm is thought to be vesselless, as is *Amborella trichopoda* (Amborellaceae), at the base of the extant angiosperm tree (Soltis and Soltis 2004). The subsequent origin of vessels is usually considered to be an important part of the angiosperm success story. However, vessels in angiosperms apparently arose long before major radiations, and the vesselless condition persists in two otherwise derived lineages, the Winteraceae (five genera, 65 species) and Trochodendrales (two monotypic families, Trochodendraceae and Tetracentraceae; Young 1981; Doyle 2000; Feild et al. 2002; Feild and Arens 2005). This pattern suggests that the vesselless condition may not be in all ways hydraulically inferior to at least the more "primitive" vessel-bearing situation. Just how inefficient is vesselless angiosperm wood for transporting water? And how vulnerable is it to cavitation by water stress? Although the anatomy of vesselless wood has been well studied (Bailey 1953; Carlquist 1975, 1983, 1987, 1988, 1990, 1992*a*, 1992*b*), until relatively recently, its functional properties have attracted less attention (Feild and Holbrook 2000; Feild et al. 2000, 2002; Feild and Arens 2005).

Our previous work on eudicots and conifers (Pittermann et al. 2005, 2006*a*, 2006*b*; Hacke et al. 2006; Sperry et al. 2006) provides an explicit hypothesis for the magnitude of flow resistance in vesselless angiosperms. We predicted that angiosperm tracheids should be ca. 38 times more resistant to flow per diameter and per length than either conifer tracheids or eudicot vessels (Pittermann et al. 2005). The prediction was based on angiosperm tracheids having the same shape and pit frequency as conifer tracheids but having angiosperm pit membranes instead of the torus-margo membranes of conifers. The homogenous, microporous pit membranes between angiosperm vessels of eudicots had ca. 60 times higher area-specific flow resistance than the torus-margo membrane. Assuming the same high resistance for intertracheid pits predicts the 38-fold greater resistance of the angiosperm tracheid. The high resistance hypothesized for angiosperm tracheids suggests a tremendous advantage to vessel evolution—decreasing resistance per unit length by spacing high-resistance endwall pitting much farther apart. In contrast, conifers achieved the

[1] Author for correspondence; e-mail j.sperry@utah.edu.

Manuscript received December 2006; revised manuscript received April 2007.

Table 1

Species, Collecting Locale, Habitat, Growth Form, and the Fraction of the Tracheid Wall Area Occupied by Intertracheid Pits (F_P)

Species	Abbreviation	Region, elevation, and lat., long.	Habitat and growth form	$F_P \pm$ SE
Amborellaceae:				
Amborella trichopoda Baill.	ATR	New Caledonia, near Sarramea, slopes of Plateau de Dogny; 650 m; 21°37′13.4″S, 165°52′.59″E	Tropical montane cloud forest; understory-subcanopy shrub	.072 ± .005
Trochodendrales:				
Tetracentron sinense Oliver	TSI	Berkeley, California, Berkeley Botanical Garden; small open-grown tree	Native to SW China; broad-leaved evergreen-mixed deciduous forests; 1100–3500 m, tree to 40 m	.159 ± .009
Trochodendron aralioides Seibold & Zucc.	TAR	Japan, vicinity of Kyoto, Kuta experimental forest; 500 m	Temperate broad-leaf forest; evergreen riparian tree	.180 ± .006
Winteraceae:				
Bubbia queenslandiana Vink	BQU	Australia, northern Queensland, Main Coast Range; 867 m; 16°35′11.7″S, 145°17′50.6″E	Tropical montane cloud forest; understory-subcanopy treelet to small tree	.057 ± .006
Bubbia semecarpoides (F. Muell.) B. L. Burtt	BSE	Australia, northern Queensland, Kuranda Range; 500 m; 16°50′13.4″S, 145°40′20.6″E	Tropical montane cloud forest; understory-subcanopy tree	.064 ± .007
Drimys granadensis L.f.	DRI	Costa Rica, Heredia Province, Volcan Barva; 2300 m; 10°06′45.7″N, 84°07′16.6″W	Tropical montane cloud forest; normally an understory to subcanopy treelet; fencerow trees were collected	.063 ± .004
Drimys winteri J. R. Forst. & G. Forst	DWI	Chile, Coquimbo Region; 550 m; 30°40′30″S, 71°40′30″W	Same as *D. granadensis*, except temperate forest	.077 ± .004
Pseudowintera axillaris (J. R. Forst. & G. Forst.) Dandy	PAX	New Zealand, NW end of S. island, Wakamarama Range; 350 m; 40°48′28.8″S, 172°28′53.5″E	Warm temperate lowland and lower montane forest; understory shrub	.045 ± .004
Pseudowintera colorata (Raoul) Dandy	PCO	New Zealand, west coast of S. island; 140 m; 42°52′30.8″S, 171°10′.14″E	Warm temperate lowland to higher montane forest, common in disturbed areas; small tree	.053 ± .004
Pseudowintera traversii (Buchan.) Dandy	PTR	New Zealand, NW end of S. island, Wakamarama Range; 900 m; 40°48′01.6″S, 172°27′47.1″E	Montane forest margins and scrub; small compact shrub	.062 ± .004
Tasmannia insipida R. Br. ex DC.	TIN	Australia, northern Queensland, Main Coast Range; 1080 m; 16°31′21.9″S, 145°15′56.7″E	Broad-leaved tropical rain forest; understory tree	.063 ± .006
Tasmannia insipida R. Br. ex DC.	TIS	Australia, northern New South Wales, Main Range Nat'l Park. 700 m. 28°17′32.1″S, 152°26′38.3″E	Broad-leaved tropical rain forest; understory tree	.060 ± .006
Tasmannia stipitata (Vick.) A. C. Sm.	TST	Australia, northern New South Wales, Forestland State Forest; 1050 m; 29°12′47.0″S, 152°07′.67″E	Tall moist eucalypt forest and rain forest; erect understory shrub	.076 ± .006
Tasmannia membranea (R. Muell.) A. C. Sm.	TME	Australia, northern Queensland, Bartle Frere peak; 1500 m; 17°23′9.9″S, 145°48′23.4″E	Tropical montane cloud forest; understory-subcanopy treelet to small tree	.063 ± .004

Table 1

(*Continued*)

Species	Abbreviation	Region, elevation, and lat., long.	Habitat and growth form	$F_P \pm$ SE
Tasmannia sp. (probably *Tasmannia purpurescens*)	TSP	Australia, greater Sydney	Cultivated tree, campus of Macquarie University, Sydney	.077 ± .006
Zygogynum baillonii Tiegh.	ZBA	New Caledonia, near Noumea, Mont Dzumac; 900 m; 22°01′47.1″S, 166°28′9.5″E	Tropical montane cloud forest; understory-subcanopy small tree	.062 ± .004
Zygogynum bicolor Tiegh.	ZBI	New Caledonia, near Sarramea, slopes of Plateau de Dogny; 860 m; 21°37′13.4″S, 165°52′.59″E	Tropical montane cloud forest; understory-subcanopy small tree	.076 ± .007
Zygogynum crassifolium (Baill.) Vink	ZCR	New Caledonia, south of Noumea, Riviere des Lacs; 180 m; 22°10′51.9″S, 166°50′49.5″E	Canopy shrub in riparian maquis scrub	.053 ± .004
Zygogynum pancherii (Baill.) Vink ssp. *pancherii*	ZPA	New Caledonia, near Noumea, Mt. Koghis slopes; 400 m; 22°10′39.6″S, 166°30′22.9″E	Tropical montane forest; subcanopy small tree	.059 ± .004
Zygogynum pommiferum Baill. ssp. *pommiferum*	ZPO	New Caledonia, near Sarramea, Table Unio (Pic Vincent); 680 m; 21°35′38.9″S, 165°46′26.7″E	Subcanopy tropical montane cloud forest; subcanopy small tree	.074 ± .008

same end by evolving torus-margo pit membranes with much lower flow resistance (Pittermann et al. 2005).

The conifer and eudicot comparison groups also predict a specific allometry between flow resistance and conduit diameter (Sperry et al. 2006). In these groups, conduit resistance standardized for length and lumen cross-sectional area (conduit area resistivity) decreased with diameter to the −2 power, a scaling that is consistent with the Hagen-Poiseuille equation. Consistent with the theory (Lancashire and Ennos 2002), this was associated with conduit length increasing with diameter to the 1.5 power across species. The evident control of conduit shape resulted in an approximately constant contribution of endwalls to the total flow resistance regardless of conduit size. The endwall contribution was 64% ± 4% in conifer tracheids and 56% ± 2% in eudicot vessels. These percentages come close to minimizing the conduit area resistivity if one assumes species-specific constraints on conduit length. Do vesselless angiosperms follow this seemingly optimal allometry, and if not, what prevents them from doing so?

The eudicot data (Hacke et al. 2006) also suggest an explicit hypothesis for the cavitation properties of vesselless angiosperms. Vesselless angiosperms should be more resistant to cavitation than eudicots because tracheids have much less total interconduit pit area per conduit than vessels. This prediction is based on the pit area hypothesis, which states that the vulnerability to cavitation by water stress increases with the total area of interconduit pitting per conduit (Wheeler et al. 2005).

The pit area hypothesis is based on the air-seeding mechanism for cavitation by water stress (Zimmermann 1983). Negative sap pressure during water stress can cause cavitation by pulling air from embolized conduits into functional conduits through the interconduit pits (Tyree et al. 1994). Homogenous pit membranes seal the air out by capillary forces in the narrow pores of the membrane. The safety of a conduit from cavitation depends on the single largest membrane pore that will form the weakest capillary seal. According to the pit area hypothesis, the size of this largest pore is influenced by the total area of pit membrane in a conduit: the more pores that are present, by chance the larger will be the single largest pore (Hargrave et al. 1994; Choat et al. 2005). In support of the hypothesis, there is a relatively tight relationship between increasing pit area per vessel and increasing vulnerability to cavitation in the eudicot data set (Hacke et al. 2006).

The tracheids of vesselless angiosperms lack a torus, and they should obey the pit area hypothesis as eudicot vessels do. Accordingly, the small pit area to be expected in these tracheids should confer very high resistance to cavitation. If the pore size distribution in the intertracheid pit membranes is approximately similar to that in eudicot intervessel pits, we ought to be able to predict the cavitation pressure from their pit area based on the relationship seen in eudicots.

To test these hypotheses of flow resistance and cavitation pressure in vesselless angiosperms, we measured these parameters on the branch wood of 19 vesselless species from three groups: Amborellaceae (one species), Trochodendrales (two species), and Winteraceae (16 species). We also evaluated whether these vesselless species show a trade-off between increasing resistance to cavitation on the one hand and increasing flow resistance or wood density on the other.

Material and Methods

Plant Material

Species, collecting locale, and habitat are listed in table 1. Collection of the material was often assisted by an expert in

the regional flora (see "Acknowledgments"). In all but two cases (*Tasmannia* sp., *Tetracentron sinense*), plants were from their native habitats. Stem pieces at least 20 cm long and ca. 0.8–1.5 cm thick and lacking major side branches were cut from one or more trees from a single population. Care was taken to avoid senescing or otherwise unhealthy material. Herbarium vouchers were made for most species and filed in J. S. Sperry's collection. Where necessary, identification was confirmed by botanical experts ("Acknowledgments") and the herbarium study. The *Tasmannia* sp. collected from the campus of Macquarrie University was tentatively identified as *Tasmannia purpurescens*, but this was not confirmed because the tree died in a heat wave. One species, *Tasmannia insipida*, is represented twice, but from very distant populations: one sample was from an apparently disjunct population in northern Queensland (Australia), and the other was from the heart of its range in New South Wales. By necessity, most of our vesselless species (16 of 19) came from the most diverse vesselless family, the Winteraceae.

After collection, stems were wrapped in plastic bags and either Express Mailed or hand-carried to J. S. Sperry's laboratory at the University of Utah, where their hydraulic properties were measured as soon as possible. In general, this was within 2–3 wk of collection. During storage, stem surfaces were kept dry to avoid fungal growth, and material was refrigerated when possible. On two occasions, the USDA inspection process created unusually long delays and the stems were not measured until nearly 4 wk after collection. However, we noticed no anomalous hydraulic behavior in any stems regardless of storage time. Dye perfusions showed continuous circumferential staining, with sapwood extending from cambium to pith in nearly every stem and species. In all species, conductivity showed similar time courses and vulnerability curves showed similar variability between stems of a species. Extensive anatomical observation of each species indicated no blockage of tracheids from fungal growth or other causes. The consistent behavior and appearance of the material suggested no effect of different storage times on the results.

Most data points represent species means based on measurements of six stems per species. Minimum flow resistance (in absence of any reversible embolism) and anatomical parameters were measured on the same set of six stems. Another set of six stems was required for cavitation "vulnerability curves," and a final set of five to six stems was used for silicone injections to estimate tracheid lengths. This made for a minimum collection size of 17 stems per species. Additional material was required for air-permeability experiments and scanning electron microscopy (SEM) observations made on a subset of species.

Flow Resistance and Anatomy

Six stems per species were cut to 14.5-cm lengths underwater and immediately flushed for 30–45 min with 20 mM KCl solution in deionized water at ca. 75 kPa to remove any reversible embolism. Stems were fitted to a tubing system where hydraulic resistivity of the same 20 mM KCl solution flowing through the stem was measured. The KCl solution was used to control for ionic effects on flow resistance (Zwieniecki et al. 2001). Resistivity (symbolized by uppercase R) was defined as the flow resistance (pressure difference per volume flow rate, symbolized by lowercase r) per length (pressure gradient per volume flow rate). Resistivity is the reciprocal of conductivity; we use both terms as a matter of mathematical or graphical convenience. Resistivity was based on the net flow rate, which was the total flow under a hydraulic head of 4–5 kPa minus the usually negative "background" flow in the absence of a difference in hydraulic head across the stem. Background flow was measured before and after the pressurized flow, with the average used to calculate the net flow. Each of these three flow measurements was the average of six successive 10-s measurements, with the flow rate monitored gravimetrically using an electronic balance. A single resistivity measurement, including the installment of the stem, took less than 15 min. Resistivity was corrected to 20°C to standardize for temperature-dependent viscosity effects (solution temperature was a few degrees higher). After the resistivity measurement, safranin dye (0.1%–0.05% w/w) was siphoned through the stems to stain functional xylem. In most stems, all xylem was functional. The cross-sectional area of stained xylem was measured at the center of the stem and multiplied by the resistivity to give a "sapwood area resistivity" symbolized as R_{Xa} (see table 2 for list of parameter definitions, abbreviations, and units).

The value of R_{Xa} depends on the number of conduits per sapwood area, conduit diameter and length, and the properties of interconduit pitting. To break down R_{Xa} into these components, we adopted the same methods used for the eudicot and conifer studies. These studies should be consulted for more detailed presentations of equations and assumptions (Hacke et al. 2006; Pittermann et al. 2006*a*). Measurements of the lumen number and cross-sectional area per sapwood

Table 2

Definition of Parameters, Abbreviations, and Units Used in Text

Abbreviation	Definition	Unit
A_P	Total area of interconduit pits per conduit	mm^2
A_P*	A_P where tracheid length is from silicone/Uvitex injections	mm^2
D	Average conduit diameter of a species, corresponds to R_L	μm
F_P	Fraction of conduit wall surface area occupied by interconduit pits	None
L	Average conduit length	mm
r_P	Flow resistance through pits on membrane area–specific basis	MPa s m^{-1}
r_W	Average flow resistance across one endwall	MPa s m^{-3}
R_C	Average conduit resistivity	MPa s m^{-4}
R_W	Average conduit endwall resistivity	MPa s m^{-4}
R_L	Average conduit lumen resistivity	MPa s m^{-4}
R_{Ca}	Lumen area–specific flow resistivity of xylem	MPa s m^{-2}
R_{Xa}	Sapwood area–specific flow resistivity of xylem	MPa s m^{-2}

Note. Resistance is defined as the pressure difference per volume flow rate and is not standardized for length of the flow path. Resistivity is pressure gradient per volume flow rate and is standardized for length. Both resistance and resistivity can be expressed on a cross-sectional-area basis.

area were made on the same stems measured for R_{Xa} (mean of 10 subsamples per stem). The R_{Xa} value multiplied by the average conduit number per sapwood area gave the average conduit resistivity, symbolized as R_C. The average lumen resistivity (R_L, at 20°C) for the stem was determined from lumen diameter measurements according to the Hagen-Poiseuille equation. We used the diameter (D) corresponding to R_L to represent the average tracheid diameter per stem. The R_C multiplied by the corresponding lumen area (from D, assuming a square lumen) gave the average conduit area resistivity, or R_{Ca}.

Assuming that lumen and endwall resistances are in a series, we estimated the average endwall resistivity (R_W) as the conduit resistivity minus the Hagen-Poiseuille lumen resistivity ($R_W = R_C - R_L$). Each parameter was determined individually for the six stems to estimate a standard error for the species.

The endwall resistivity, R_W, was broken down into its anatomical components. The endwall was defined as the area of overlap between tracheids that links them into longitudinal files. We assumed that, on average, one-half of the tracheid overlaps with upstream tracheids and the other half overlaps with downstream ones. Accordingly, the average distance between endwalls equaled half of the average tracheid length (Lancashire and Ennos 2002). The average resistance of an endwall, r_w, was estimated as R_W multiplied by the average distance between endwalls. Tracheid length was measured in macerations, averaging from ca. 80 to 140 tracheids per species. The endwall resistance in turn was expressed on the basis of the endwall pit dimensions. The pit area resistance (r_P) was defined as the pit resistance on a membrane surface area basis. Even though the pit resistance was standardized for area, it was not standardized for the path length from lumen to lumen, so it is a resistance rather than a resistivity in our terminology (table 2). The endwall resistance is the r_P divided by the pit membrane area per endwall: $r_w = 2r_P/A_P$, where A_P represents the total interconduit pit area per conduit (both endwalls together). We measured A_P and calculated r_P from r_W.

The intertracheid pit area per conduit (A_P) used to calculate r_P was estimated from the same macerations used to measure tracheid length. From the macerated tracheids, we determined the average fraction of tracheid wall surface area occupied by intertracheid pits (F_P). Intertracheid pits were rare on tangential walls and essentially confined to the radial walls. The fraction of the radial wall occupied by intertracheid pits was measured on typically 12–15 tracheids per species. The fraction was divided by 2 (to account for the nonpitted tangential walls) to estimate F_P. The average A_P per species was then calculated as F_P times the average surface area of a tracheid per species ($=4DL$, where L is average tracheid length). In one species, *Trochodendron aralioides*, where latewood and earlywood were rather distinct and latewood was abundant, the pitting pattern differed so dramatically between the corresponding tracheids that we weighted the F_P value according to the relative fraction of intertracheid contact in earlywood and latewood. Intertracheid contact was quantified in cross section as the total perimeter of tracheids in contact with each other in a growth ring, and the fraction in earlywood and latewood was calculated. The weighted F_P equaled the earlywood F_P times the early-wood contact fraction plus the latewood F_P times the latewood contact fraction.

Standard errors were estimated directly from multiple samples for most parameters (R_{Xa}, R_{Ca}, R_C, R_L, R_W, F_P, L, and D). For those parameters that could be calculated only from species means (r_P, A_P, r_W), errors were propagated through the various equations. All parameters are averages for all functional conduits within the branch xylem of the species.

Silicone Injections

To check for "cryptic vessels" in these vesselless woods (Feild et al. 2000), we also measured conduit lengths by the silicone injection method as described in detail previously (Wheeler et al. 2005). Cryptic vessels would result if intertracheid pit membranes were missing or contained exceptionally large pores. The silicone has been shown to penetrate margo-sized pores in conifers, which often exceed 0.3 μm in span, but not the much smaller pores of intervessel pit membranes (Andre 2005). Stems were flushed to remove embolism and then injected at 25–50 kPa overnight with a 10 : 1 silicone-hardener mixture (RTV-141, Rhodia, Cranbury, NJ).

Initially, we colored the silicone with red pigment (Silastic LSPRD11, Dow Corning, Kendallville, IN) as in our previous work. However, we found that the average particle size was too large (0.60 ± 0.11 μm) to potentially travel with the silicone through tracheid endwalls with large-pit membrane pores. Species were reinjected with a soluble fluorescent whitening agent (Ciba Uvitex OB, Ciba Specialty Chemicals, Tarrytown, NY). The Uvitex was dissolved in chloroform (1% w/w), and one drop of silicone-hardener mix per gram was added. The solution was mixed quickly to avoid evaporation and precipitation of the Uvitex. The silicone fluoresced brightly and served as a convenient marker for filled conduits, which were otherwise clear in microscope sections.

Injected stems were sectioned at 1, 2, 3, 6, and 10 mm and occasionally at longer intervals from the injected surface, and the number of filled conduits per cross-sectional area were counted. These counts formed the basis for calculating the conduit length distribution.

For vessels, which have a much more spread-out length distribution than tracheids, we have used a single-parameter exponential decay function to fit the decrease in the density of silicone-filled vessels (N_L) with distance (L) from injection: $N_L = N_0 e^{(-kL)}$, where $N_0 = N_L$ at $L = 0$ and k is the best-fit extinction coefficient. The second derivative of this equation multiplied by L/N_0 gives the fraction of injected conduits of length L (Cohen et al. 2003). Tracheids, however, have a much shorter length distribution, and an artifact of this function was to give significant fractions of tracheids that were unrealistically short—of just a few tenths of a millimeter, for example. The artifact arises because the rate of decay for the function increases monotonically as L goes to 0. The function also forces the distribution to be strongly short skewed, which is appropriate for vessels (Zimmermann and Jeje 1981) but not necessarily so for tracheids. To better represent tracheid distributions, we used a Weibull function to fit the decline in silicone-filled tracheids with distance L:

$$N_L = N_0 e^{(-kL)^c}, \quad (1)$$

where c is a second curve-fitting parameter. For best-fit $c > 1$ (nearly always the case), the rate of decay does not increase

monotonically as L goes to 0. The second derivative multiplied by L/N_0 gives the fraction of vessels of length L:

$$F_L = ckL^{c-1}e^{(-kL)^c}(ckL^c + 1 - c), \quad (2)$$

and the integral from $L = 0$ to ∞ of F_L gives 1. However, for the usual case where $c > 1$, F_L becomes negative below a minimum length $L_{min} = [(c-1)/ck]^{1/c}$. We used L_{min} to represent the minimum tracheid length and adjusted F_L from equation (2) accordingly by dividing it by the integral of equation (2) from L_{min} to ∞. The Weibull cannot be integrated analytically, so numerical methods were used. Typical tracheid-length distributions using this method were still short skewed, although much less so than vessel distributions. Except for comparison with maceration data (fig. 6), we represented the silicone-based length distribution using the log-transformed mean.

Cavitation "Vulnerability Curves" and Evaluation of the Pit Area Hypothesis

Vulnerability curves show the loss of hydraulic conductivity with increasingly negative xylem pressure. Curves for six stems per species were measured with the standard centrifugal force method (Alder et al. 1997). Stems were flushed and measured for conductivity (reciprocal of resistivity) as previously described. Measurements were repeated after stems were spun in a custom-designed centrifuge rotor to progressively more negative xylem pressures. Stems were held at each pressure for 15 min to ensure complete cavitation before being taken out of the rotor and directly remeasured for conductivity (Alder et al. 1997). The percentage loss in conductivity from the original value was plotted versus the negative pressure to give the vulnerability curve. Curves were fit with a Weibull function for each stem, and mean cavitation pressure was

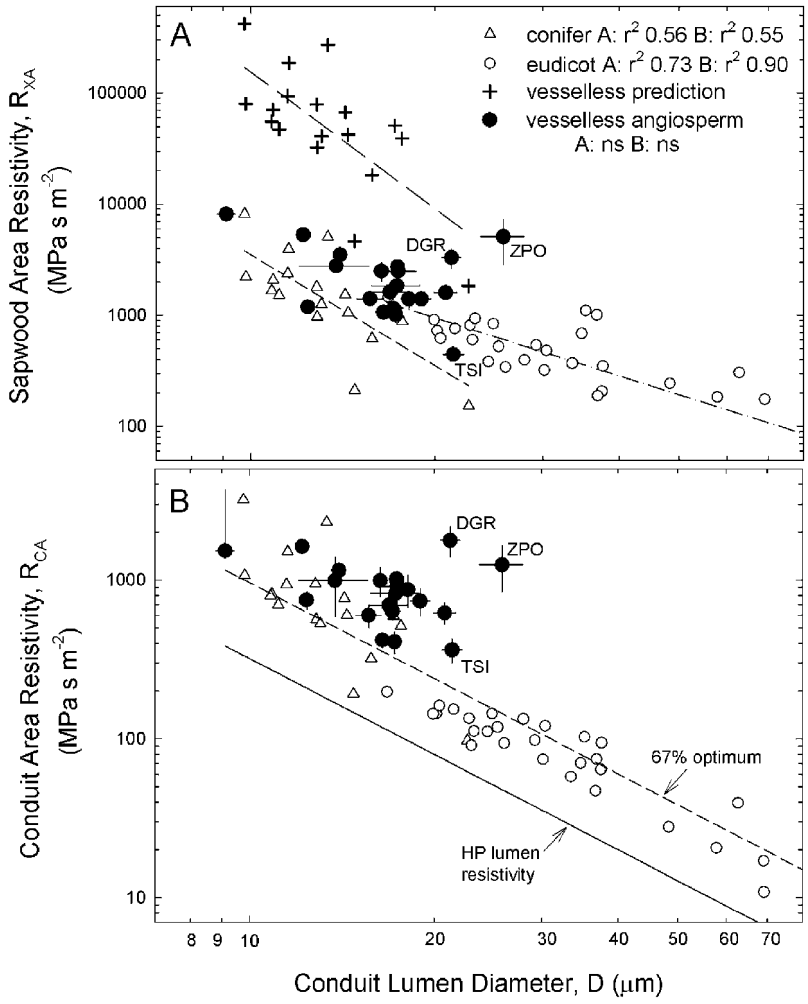

Fig. 1 Xylem flow resistivity on a sapwood (*A*) and conduit lumen (*B*) area basis versus average conduit lumen diameter. Each data point is a species mean; species abbreviations from table 1. Conifer and eudicot branch wood data are from Hacke et al. (2006) and Pittermann et al. (2006*a*). Predicted values for vesselless angiosperms in *A* (crosses, dashed line) are based on conifer tracheid geometry and eudicot intervessel pit resistance (Pittermann et al. 2005). In contrast to conifers and eudicots, vesselless angiosperms show no decrease in resistivity with wider diameter (species means ± SE). Solid diagonal in *B* is the Hagen-Poiseuille area resistivity for an unobstructed conduit lumen. Dashed diagonal in *B* represents conduits where endwalls contribute 67% of the total resistivity. This approximates the scaling seen in conifers and eudicots and also minimizes the area resistivity, assuming each species has a fixed conduit length (Sperry et al. 2006).

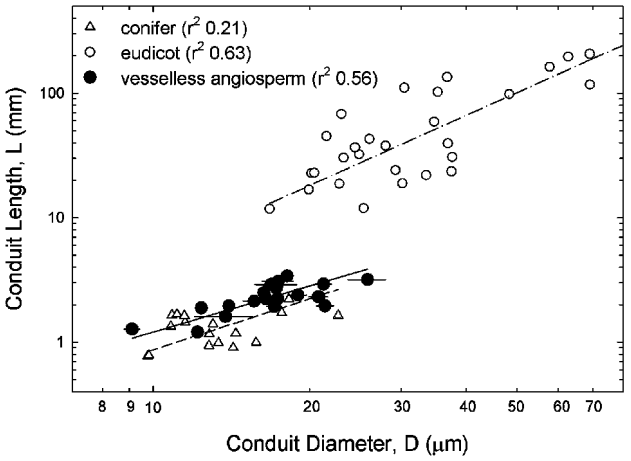

Fig. 2 Log-log scaling of average conduit length with average conduit diameter. Data points are species means. Eudicot and conifer branch wood data from Hacke et al. (2006) and Pittermann et al. (2006*a*). Vessel lengths are log-transformed means of short-skewed vessel-length distributions. Tracheid lengths are arithmetic means from macerations. Reduced major axis regression lines are shown. Slopes are not different from the 1.5 value required for proportionality of endwall and lumen resistivity, assuming that pit area resistance and pit area per conduit surface area are independent of conduit size (Lancashire and Ennos 2002).

calculated from the best fit. Average mean cavitation pressure was based on $n = 6$ stem means per species.

To evaluate the pit area hypothesis, we compared the mean cavitation pressure with the mean pit area per cavitating conduit (A_P). Normally, this would be the same A_P per tracheid used to calculate the tracheid pit area resistance (r_P); this was based on the length of tracheids measured in macerations. However, as explained in "Results," the conduit lengths calculated from silicone/Uvitex injections were often longer than the actual tracheid. Many tracheids were connected by pit membranes with holes large enough to pass the silicone, which is normally stopped by pit membranes without the torus-margo structure. Any pit membrane that lacks a torus and is permeable to silicone should also have a very low air-seeding pressure. A series of tracheids linked by such perforated pit membranes would be expected to cavitate as a single unit. To test whether the cavitation pressure of this multitracheid unit is linked to its total pit area, the pit area is best estimated from the length of the multitracheid unit. For that reason, we used the silicone/Uvitex-based lengths for calculating the A_P associated with cavitation pressure. We designate this parameter as A_P* to distinguish it from the A_P per tracheid calculated from maceration-based tracheid length.

Wood Density

To determine whether resistance to cavitation in vesselless angiosperms increases with wood density as seen for conifers and eudicots (Hacke et al. 2001), we measured the dry weight per fresh volume of secondary xylem samples whittled from the same stems used for the vulnerability curves. Measurement details are reported by Hacke et al. (2001).

Air-Permeability Experiments

To test for a link between pit membrane permeability to air and cavitation pressure, we did air-injection experiments on a subset of species (*Zygogynum pancherii*, *Zygogynum bicolor*, *Zygogynum pommiferum*, *Amborella trichopoda*, *Tasmannia insipida* [New South Wales population], *Pseudowintera axillaries*, *Pseudowintera traversii*, *Bubbia semecarpoides*, *Bubbia queenslandiana*, *Trochodendron aralioides*, and *Drimys granadensis*). Dowels of secondary xylem were whittled from stems and attached at one end to a compressed nitrogen source. Dowels were ca. 2.2–2.5 cm long and ca. 3–5 mm in diameter. Gas pressure was raised stepwise and the flow rate of gas measured by its rate of displacement of water from a reservoir onto an electronic balance. The flow rate was converted to an approximate pneumatic conductivity by dividing it by the air-pressure gradient across the dowel. The conductivity was approximate because it did not take into account the compressibility of air. Dowels were used rather than entire stems to avoid air penetration through the pith. Typically, there was a pressure threshold below which no measurable airflow occurred and above which the airflow increased abruptly. An "air-entry" pressure across the dowel was calculated from plots of pneumatic conductivity versus gas pressure using the extrapolation method of Sparks and Black (1999). The air-entry pressure represents the minimum air-seeding pressure for the intertracheid pit membranes. The average air-entry pressure calculated from injections was compared with the average air-entry pressure calculated from stem vulnerability curves using the same extrapolation method. To a first approximation, the two should agree if cavitation is caused by air-seeding across pit membranes.

Scanning Electron Microscopy Observations

A subset of species (*A. trichopoda*, *T. aralioides*, *D. granadensis*, *P. traversii*, and *Z. pancherii*) were examined in the SEM to

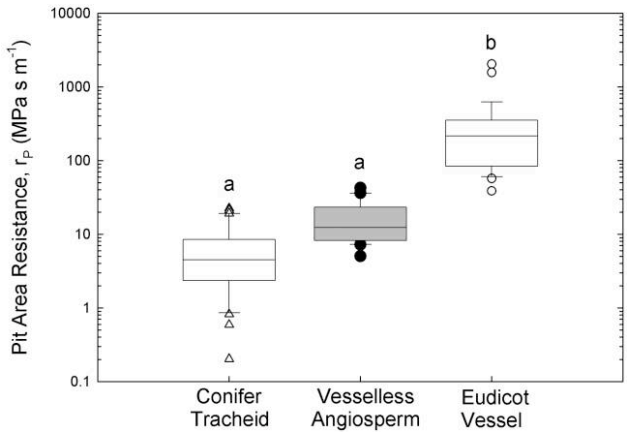

Fig. 3 Flow resistance across pits on a pit membrane surface area basis. Boxes mark the twenty-fifth to seventy-fifth percentile range and the median value (middle horizontal bar) for all species means for the three xylem types. Vertical lines show tenth to ninetieth percentile range, with outlying points as symbols. Means sharing the same letter were not significantly different (one-way ANOVA followed by least significant difference test). Eudicot and conifer data from Hacke et al. (2006) and Pittermann et al. (2006*a*).

assess the porosity of the intertracheid pit membranes. For comparison, we also include observations of intervessel pit membranes in *Trimenia neocaledonica* (Sperry et al. 2007). Wood samples were preserved in 50% ethanol and shipped to Hokkaido University, Japan, where they were prepared for microscopy by Y. Sano. Samples were prepared as described previously (Sano 2005; Sano and Jansen 2006). In brief, samples were cut into small cubes (ca. 5 mm^3) in wet condition. The blocks were air-dried after dehydration in absolute ethanol. Wood surfaces to be observed were exposed by splitting (cracking) with a razor blade. They were coated with platinum by vacuum evaporation (JE-4, Jeol, Tokyo) and viewed with a field-emission scanning electron microscope (JSM-6301F, Jeol) at an accelerating voltage of 2.5 kV.

Statistics

Allometric scaling of conduit length with diameter was determined from reduced major axis regression (Niklas 1994) rather than least squares regression (fig. 2) because neither dimension was independently controlled. Probability threshold for standard statistical tests of significance for regression lines and mean differences was 0.05 unless noted. We used SPSS software for these tests (SPSS, Chicago).

Results

Sapwood area resistivities (R_{Xa}) and conduit area resistivities (R_{Ca}) of vesselless angiosperms were considerably less than what we had predicted from conifer tracheid dimensions and eudicot pit resistances (fig. 1, cf. filled circles with crosses). Contributing to this lower-than-expected resistivity was the fact that angiosperm tracheids tended to be longer for their diameters than conifer tracheids, although not by a statistically significant degree (fig. 2). Longer tracheids would tend to minimize the conduit endwall contribution. The main reason for the low resistivity, however, was that the estimated pit area resistance for angiosperm tracheids (fig. 3) was much lower (mean ± SE: 16 ± 2 MPa s m^{-1}) than the eudicot average (336 ± 81 MPa s m^{-1}; Hacke et al. 2006) and not significantly different from the torus-margo value for conifers (5.7 ± 1.3 MPa s m^{-1}; Pittermann et al. 2005). The fraction of tracheid wall pitted was no different between angiosperm ($F_P = 0.075 \pm 0.008$; table 1) and conifer tracheids ($F_P = 0.086 \pm 0.008$; Pittermann et al. 2006*a*).

Another departure from expectation was that R_{Ca} for vesselless angiosperms did not decrease with increasing tracheid diameter to the −2 power as was statistically the case in conifer tracheids and also eudicot vessels (fig. 1*B*; Sperry et al. 2006). Remarkably, R_{Ca} for vesselless angiosperms did not decrease at all with increasing diameter, and two of the species with the largest tracheids (*Zygogynum pommiferum* and *Drimys granadensis*) had R_{Ca} values high enough to be within the predicted range (fig. 1*B*, *ZPO*, *DGR*).

Concordant with R_{Ca} being independent of tracheid diameter in vesselless angiosperms, the percentage of the xylem resistivity in tracheid endwalls increased significantly with tracheid diameter ($r^2 = 0.38$; data not shown), from 64% for the species with the narrowest tracheids (*Pseudowintera traversii*; $D = 9.1$ μm) to 92% for the species with the widest tracheids (*Z. pommiferum*; $D = 26$ μm). Overall, 77% ± 2% of the xylem resistivity was in the endwall. This contrasts with conifers, where endwall resistivity was independent of tracheid size and averaged 64% ± 4% overall (Pittermann et al. 2006*a*).

The increase in percentage of endwall resistivity with diameter could not be attributed to tracheid allometry. Figure 2 shows that the across-species allometry of length and diameter in angiosperm tracheids was very similar to conifer tracheids. The slope of the reduced major axis regression was not different from 1.5 in either case ($P \gg 0.05$). This value maintains a size-independent endwall percentage if the fraction of tracheid wall that is pitted (F_P) and pit area resistance (r_P) do not change systematically with diameter (Lancashire and Ennos 2002). This was true for F_P (data not shown), but it was not true for r_P.

The value of r_P increased strongly with increasing diameter and pit area (fig. 4), the major exception being in *Tetracentron sinense* (fig. 4, *TSI*). The trend for increasing pit area resistance in some of the species with larger tracheids (fig. 4, e.g., *ZPO*, *DGR*) made the endwall resistivity increasingly limiting and prevented the overall tracheid area resistivity from decreasing with diameter (fig. 1*B*).

The SEM observations indicated a general tendency for more porous pit membranes to be associated with lower r_P (fig. 5). Of the five species examined in the SEM (labeled in fig. 4), the most conspicuously porous membranes were from species with the lower pit area resistances: *P. traversii* ($r_P = 11.1 \pm 1.4$ MPa s m^{-1}; fig. 5*A*), *Trochodendron aralioides* ($r_P = 24.4 \pm 4.1$ MPa s m^{-1}; fig. 5*B*), and *Amborella trichopoda* ($r_P = 22.9 \pm 5.8$ MPa s m^{-1}; fig. 5*C*). Carlquist (1992*a*) has noted the exceptionally porous membranes in *T. sinense* (his fig. 34), consistent with its very low pit resistance ($r_P = 7.6 \pm 1.4$ MPa s m^{-1}).

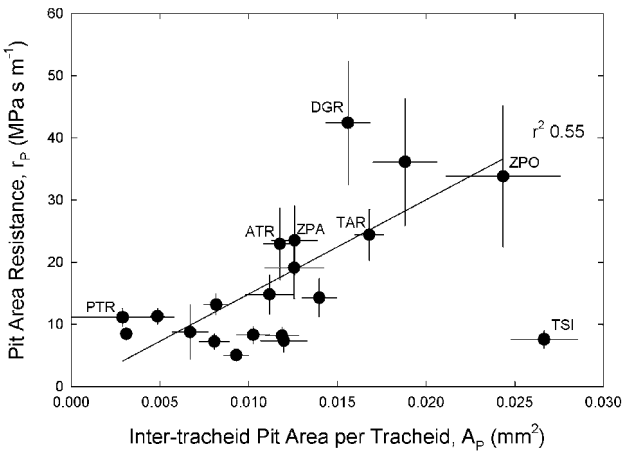

Fig. 4 Pit resistance standardized for pit membrane area versus intertracheid pit area per tracheid. Pit areas were based on tracheid length measured in macerations. Species means ± SE; abbreviations from table 1. Larger tracheids with larger pit areas (e.g., *DGR*, *ZPO*) generally had higher area-specific pit resistances. Area-specific pit resistance also increased with tracheid diameter (data not shown). A notable outlier not included in the regression is *Tetracentron sinense* (*TSI*). Other labeled species were viewed in the scanning electron microscope (fig. 5).

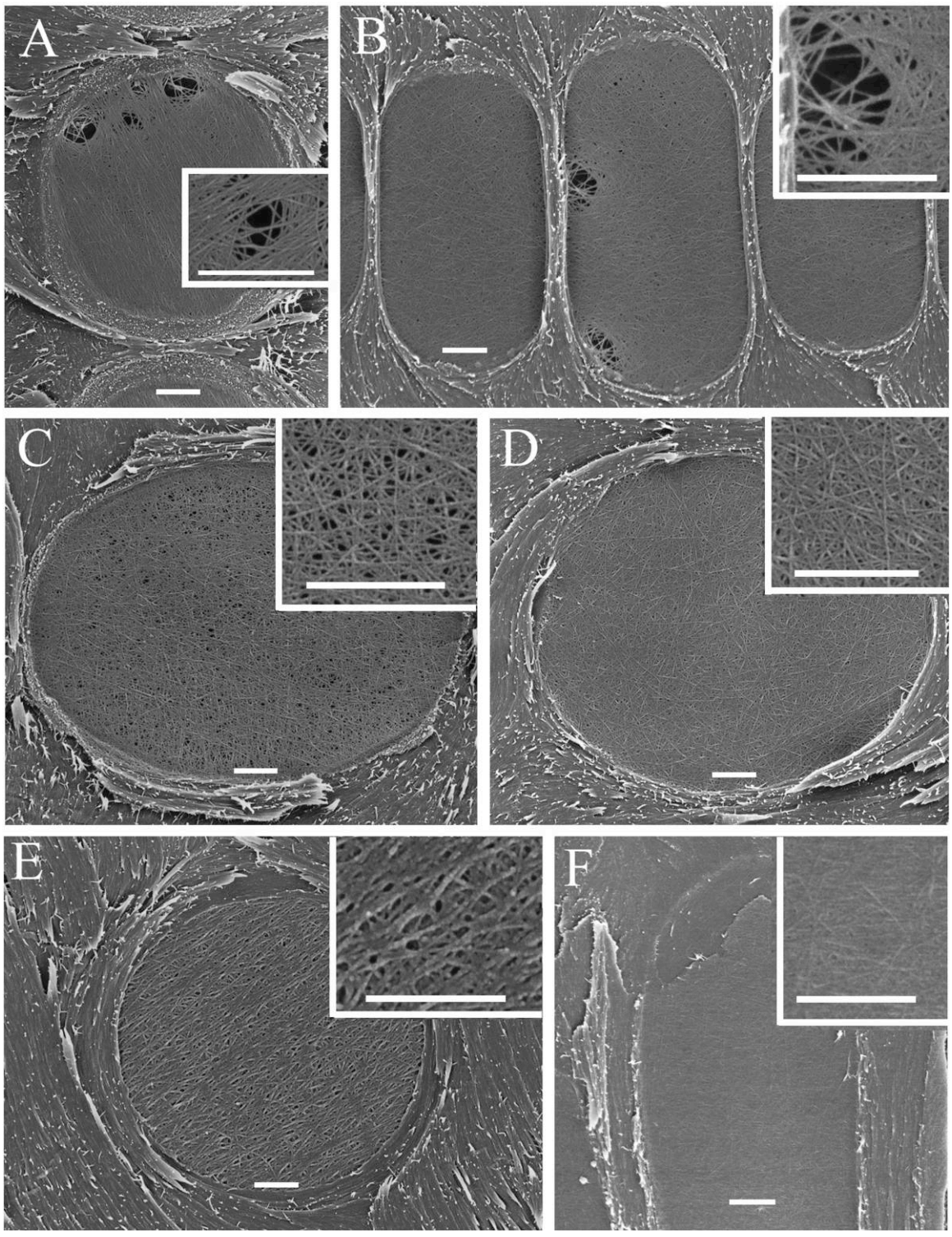

Fig. 5 Scanning electron microscope images of intertracheid (*A–E*) and intervessel (*F*) pit membranes. Insets show magnified sections of membrane. Scale bar = 1 μm in all cases; micrographs taken at between ×7000 (*D*) and ×10,000 (*A*) magnification. *A*, *Pseudowintera traversii*. *B*, *Trochodendron aralioides*. *C*, *Amborella trichopoda*. *D*, *Zygogynum pancherii*. *E*, *Drimys granadensis*. *F*, *Trimenia neocaledonica*.

In contrast, pit membranes from the species with the highest pit resistance, *Drimys granadensis*, had relatively small pores ($r_P = 42 \pm 9.9$ MPa s m^{-1}; fig. 5*E*). By comparison, pores are often not visible in the SEM for intervessel pit membranes of many vessel-bearing species such as *Trimenia neocaledonica* (fig. 5*F*). Not fitting this correspondence between observed porosity and pit resistance was *Zygogynum pancherii*, which had relatively low pit resistance ($r_P = 23.5 \pm 5.6$ MPa s m^{-1}; fig. 4) but barely visible membrane pores (fig. 5*D*).

The silicone injections also provided indirect evidence for relatively large pores in intertracheid pit membranes of at least some of the vesselless species (fig. 6). When the red pigment of large particle size (0.60 ± 0.11 μm) was used with silicone, mean tracheid length was similar whether calculated from the injections or measured directly from macerations (fig. 6, open circles; regression not different from 1 : 1 line). However, when the soluble Uvitex dye was used, mean tracheid length measured by injection exceeded the maceration measurement in several species, especially so in *A. trichopoda*, *Bubbia queenslandiana*, *Zygogynum baillonii*, *Tasmannia membranea*, and *Zygogynum bicolor* (fig. 6, filled circles, abbreviations). On average, the mean tracheid length from the silicone/Uvitex injection was 1.5 ± 0.1 times longer than the mean from macerations, ranging from just over 1.0 in several species to a high of 2.9 in *A. trichopoda*.

Vulnerability curves of the vesselless taxa were very similar in shape: a sigmoidal relationship with a well-defined cavitation threshold (fig. 7). However, there was considerable variation in the mean cavitation pressure, ranging from -1.5 ± 0.1 MPa in *T. sinense* to -5.5 ± 0.2 MPa in *P. traversii*. The grand mean for all species was -3.4 ± 0.3 MPa, indicating a surprising degree of protection from cavitation, given their generally wet and often shaded habitats (table 1). The north

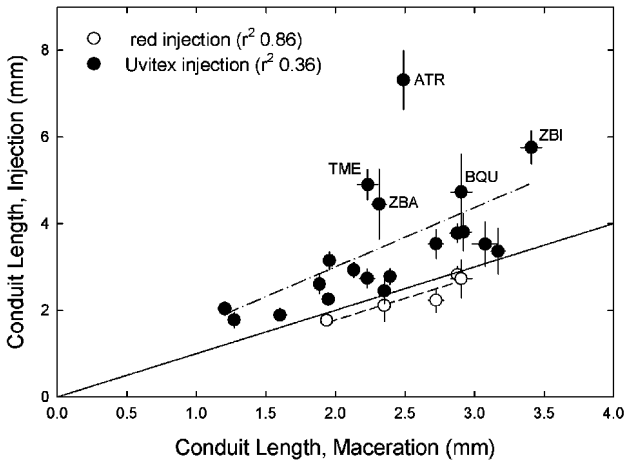

Fig. 6 Conduit lengths measured by the silicone-injection method versus by the maceration method. Solid line is 1 : 1 agreement. Data points are species means ± SE, non-log-transformed. In five species, the silicone contained a red pigment whose average particle size of ca. 0.6 μm inhibited penetration through porous intertracheid pit membranes (open symbols). All but one of these species, plus the remaining ones, were reinjected with silicone plus soluble Uvitex fluorescent dye (filled symbols). Species abbreviations from table 1.

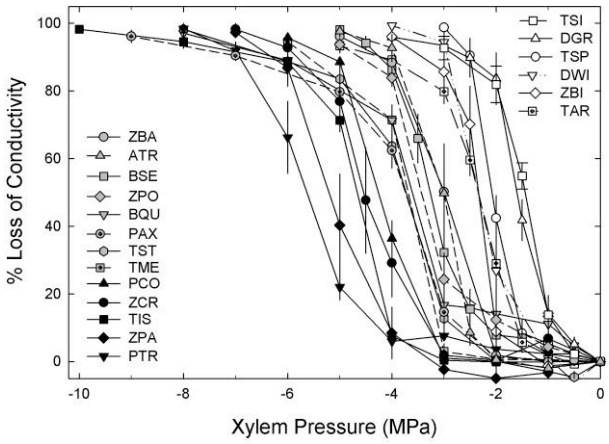

Fig. 7 Vulnerability-to-cavitation curves for vesselless taxa showing percentage loss of conductivity as a function of negative pressure. Curves are means ± SE for six stems per species. Symbols are identified from most vulnerable (top right, open symbols) to increasingly resistant (left, from top to bottom, gray and black symbols). Species abbreviations from table 1.

Queensland population of *Tasmannia insipida* is not shown but was very similar to the New South Wales population for the first half of the vulnerability curve (up to 50% loss of conductivity). However, beyond this point, the xylem was much more resistant. Because of the very different curve for this apparently disjunct Queensland population, we did not use it in further analysis but represented the cavitation resistance of the species with the New South Wales data.

Overall, the threshold cavitation pressure compared favorably with the threshold air-entry pressure for the air-injected species (fig. 8; regression confidence limits include 1 : 1 line), supporting the hypothesis that air entry through pit membranes was causing the cavitation. Species furthest from agreement were *P. traversii* and *T. aralioides*, where the average air-entry pressure was less than the cavitation threshold, and *B. queenslandiana*, which showed the opposite situation (fig. 8).

The vesselless angiosperms did appear to follow the pit area hypothesis but not in the simple way expected from the published eudicot data (fig. 9; Hacke et al. 2006). The vesselless taxa were consistent with the hypothesis because there was a significant relationship between increasing interconduit pit area (A_P* from silicone length data) and increasing vulnerability to cavitation. The slope of the log-log relationship (-1.30 ± 0.33) was no different from that of the eudicot data (-1.92 ± 0.20). Using the pit area estimated from macerations (A_P instead of A_P*) also gave a significant relationship ($r^2 = 0.45$; data not shown), with a similar slope. Notably, the vesselless taxa had substantially less total pit area per conduit for the same cavitation pressure than eudicot taxa (fig. 9). This is consistent with intertracheid pits having more porous membranes than intervessel pits (see "Discussion").

There was evidence of a trade-off between increasing resistance to cavitation and increasing sapwood area resistivity ($r^2 = 0.28$) and a significant trend ($r^2 = 0.27$; data not shown) for narrower tracheids to be more resistant to cavitation. We also found a relationship between greater wood density and

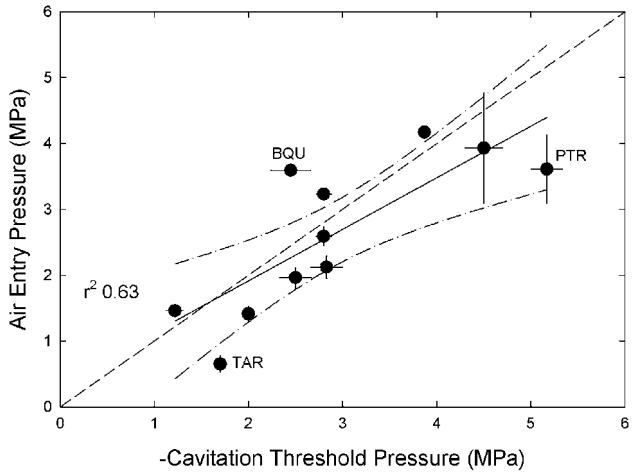

Fig. 8 Air-entry threshold measured by forcing air through dowels of wood versus the cavitation threshold determined from vulnerability curves. Threshold pressures calculated by the method of Sparks and Black (1999). Species means ± SE; abbreviations from table 1. Solid line is 1 : 1. Dashed line is regression with dot-dashed 95% confidence intervals.

cavitation resistance (fig. 10, filled symbols) as found previously for conifers (fig. 10, open symbols; Hacke et al. 2005; Pittermann et al. 2006*b*) and eudicots (not shown; Hacke et al. 2001, 2005).

Discussion

Vesselless angiosperms had more efficient xylem than expected from our calculation based on the combination of conifer tracheid geometry and eudicot intervessel pit resistance. The deviation was not a result of tracheid geometry, which was similar between conifers and vesselless angiosperms in terms of the intertracheid pit fraction and length-diameter scaling across species. The deviation occurred primarily because the intertracheid pits of vesselless angiosperms had much lower area-specific resistance than intervessel pits. The lower resistance was associated with a more porous appearance of the pit membrane under the SEM and penetration of silicone through tracheid endwalls in many species. This agrees with previous observations of exceptional porosity in the intertracheid pit membranes from some vesselless angiosperms (Carlquist 1983, 1992*a*; Feild et al. 2000; Carlquist and Schneider 2002).

The evolution of greater membrane porosity in tracheids than in vessels—whether in the form of the gymnosperm torus-margo or more irregularly dispersed as in angiosperm tracheids—would be favored by the large drop it causes in xylem flow resistance.

When pit membranes are responsible for more than 80% of xylem flow resistance, as in over half of our vesselless taxa, variation in pit membrane porosity has major consequences for transport efficiency. Such variation was apparently responsible for the surprising lack of a decrease in conduit resistivity with increasing tracheid size, deviating significantly from the second-power decline observed in conifers and eudicots (Sperry et al. 2006). Some vesselless angiosperms with larger mean tracheid diameter (*Drimys granadensis*, *Zygogynum pommiferum*, *Zygogynum baillonii*) had conduit area resistivities just as high in as species with narrower tracheids. This observation is attributed to the observed trend for increasing pit area resistance with greater intertracheid pit area, which is a proxy for tracheid size. *Tetracentron sinense* was a marked exception to this trend, exhibiting relatively wide tracheids, low pit area resistance, and the lowest conduit area resistivity of all taxa. It also has notably porous intertracheid pit membranes (Carlquist 1992*a*).

The significance of variation in pit membrane porosity and resistance within the vesselless taxa is not clear. Species or populations with lower pit membrane resistances (e.g., *T. sinense*) could be adapting or acclimating to conditions of higher transpirational stress, where a premium is placed on achieving low flow resistance. Low pit area resistance also compensates for high lumen resistance, an advantage that could explain the tendency for low pit area resistance to occur in species with narrow tracheids as seen in figure 4.

A potential constraint on the evolution of porous intertracheid pit membranes is that they will become less effective at preventing air seeding and make the tracheids more vulnerable to cavitation. The data indicate, however, that vesselless angiosperms are not plagued by excessive vulnerability to cavitation, with an average cavitation pressure of −3.4 MPa. Some, such as *Zygogynum pancherii* (mean cavitation pressure −5.1 ± 0.3 MPa) and *Tasmannia insipida* (−4.7 ± 0.1 MPa), seem especially overbuilt for their generally wet and humid understory habitats, often in montane cloud forests. Even the most vulnerable, *T. sinense* (−1.5 ± 0.1 MPa) and *D. granadensis* (−1.6 ± 0.1 MPa), are no more so than a typical riparian diffuse-porous eudicot (Pockman and Sperry 2000). Safety margins from cavitation cannot be estimated without knowing the range of xylem pressures experienced by the plants in their native habitats. The indication, however,

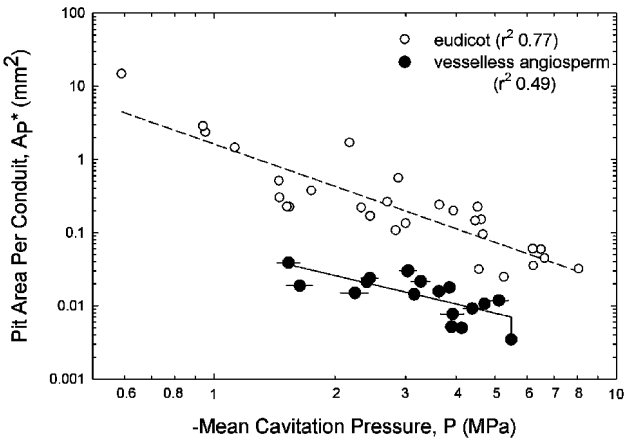

Fig. 9 Log-log scaling of interconduit pit area per conduit versus mean cavitation pressure for vesselless angiosperms (filled symbols) and compared with eudicot species (open symbols). Data points are species means ± SE for vesselless data. Pit areas for vesselless taxa based on silicone/Uvitex length data. Pit areas from maceration length data gave a very similar and significant relationship ($r^2 = 0.45$). Eudicot branch wood data from Hacke et al. (2006).

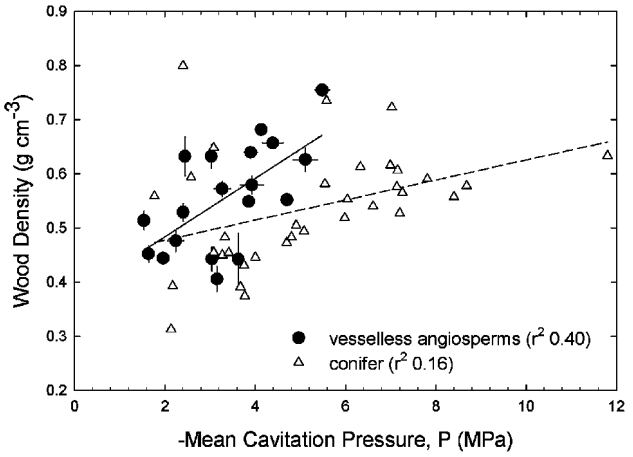

Fig. 10 Wood density versus mean cavitation pressure for vesselless angiosperms (filled symbols) and compared with conifers (open symbols). Data points are means ± SE for vesselless angiosperms. Conifer branch wood data from Pittermann et al. 2006*a* and Hacke et al. (2001, 2005).

is that vulnerability to cavitation in these vesselless taxa may not be as uniformly matched to the demands of habitat as can be the case for vessel-bearing taxa.

Luxurious, or at least very adequate, safety margins from cavitation for tracheids in spite of rather porous pit membranes are consistent with the pit area hypothesis. If angiosperm tracheids had the same small pore-size distribution in their pit membranes as eudicot vessels, they should have fallen on the same eudicot regression line in figure 9. In that case, the small pit areas of tracheids would result in cavitation pressure averaging −12 ± 1 MPa for the vesselless taxa. Such extreme resistance to cavitation would be even more unnecessary in their typically wet habitats than would the actual values. Instead, angiosperm tracheids fell on a different regression line, indicating less total pit area for the same maximum pore size and vulnerability than in eudicot vessels (fig. 9). This shift in regression lines is consistent with greater average membrane porosity in intertracheid pit membranes as compared with intervessel pit membranes. The angiosperm tracheids can get away with having more porous membranes because their small pit areas per tracheid keep the size of the largest membrane pore per tracheid within acceptable limits. They benefit from their porous membranes by a reduction in xylem flow resistance.

Some relatively vulnerable species such as *T. sinense* and *D. granadensis* have apparently pressed this hypothetical advantage more than others. The apparently comfortable safety margins in other species suggest that the trade-offs we identified between cavitation resistance, narrower tracheids, higher sapwood resistivity, and greater wood density are not uniformly important across vesselless angiosperms, many of which grow in wet, dark habitats with low transpirational stress. It is possible that greater wood density is advantageous in its own right for some species, providing benefits of greater wood strength and branch longevity. Achieving it could require narrower tracheids because of a limitation on maximum wall thickness (Pittermann et al. 2006*b*). That such narrow tracheids bring along with them an automatically greater resistance to cavitation may be ecologically less relevant.

Our estimated pit resistances are the average for all pit membranes over the length of the stem. They potentially mask considerable heterogeneity in pit membrane porosity within a branch, heterogeneity that would be predicted for the early stages of vessel evolution. If all intertracheid pit membranes became perforated, the entire tracheid network would cavitate in one disastrous event. To mitigate this risk, the perforation of pit membranes must be restricted to only a subset of intertracheid connections, initially forming "cryptic vessels" that are connected to one another by nonperforated pit membranes (Feild et al. 2000). Such a cryptic vessel would cavitate as a unit.

Our results provide some evidence for cryptic vessel formation in some of the vesselless species. The simplest example is the penetration of the silicone-Uvitex injection well beyond the length of an individual tracheid. Uvitex penetration was especially pronounced in the five species labeled in figure 6, where the mean length of a cryptic vessel averaged twice the mean length of the tracheid. Although we are not sure of the pore size threshold for silicone penetration, a conservative estimate is the 0.3–0.5-μm range, based on its penetration through the margo of conifer pits (Andre 2005). The species with the longest silicone penetration, *Amborella trichopoda*, has previously been suggested to harbor cryptic vessels (Feild et al. 2000).

The SEM observations, vulnerability curves, and air-injection experiments also suggest cryptic vessels in some species. Views of *Pseudowintera traversii* and *Trochodendron aralioides* membranes commonly revealed holes of ca. 0.4 μm (fig. 5) that would air seed at only −0.8 MPa (surface tension 0.072 Pa m, contact angle of 0°), whereas the threshold cavitation pressure (not mean) for incipient air seeding was much lower, at −5.2 and −1.7 MPa for the two species, respectively (fig. 8). The implication is that these exceptional holes were only in a subset of intertracheid pit membranes (consistent with SEM observations), representing the "perforation plates" of cryptic vessels.

Pseudowintera traversii and *T. aralioides* were also the two species that had air-entry pressure, measured directly on short 2.5-cm dowels, that was quite a bit lower (and more variable) than the cavitation threshold pressure, measured on 14.2-cm-long stems. Air would "seed" through shorter lengths at lower pressure than it would through longer lengths because of the greater chance for the longitudinal alignment of permeable pit membranes. In seven of the 11 species tested, air-entry pressure through the short dowels was less than the cavitation threshold, although the confidence limits of the overall relationship encompassed the 1 : 1 line (fig. 8). Complicating the story, however, is *Bubbia queenslandiana*. It had exceptional silicone penetration indicative of cryptic vessels (fig. 6) but was the only species that had an air-entry pressure markedly greater than the cavitation threshold (fig. 8).

Heterogeneity of pit membranes complicates the interpretation of the pit area hypothesis as well as the interpretation of SEM observations. Micrographs from species with low average pit resistance can show pores larger than required to explain air seeding, as in the case of *P. traversii* and *T. aralioides*, consistent with being perforated pit membranes of cryptic vessels. Conversely, in species with higher average pit resistance and presumably fewer or shorter cryptic vessels, SEM observations generally revealed pores smaller than the magnitude

required for air seeding. In *D. granadensis*, for example, the cavitation threshold of −1.2 MPa corresponds to a pore diameter of 0.24 μm (assuming zero contact angle). Assuming the pit area hypothesis, this would correspond to the single largest pore in the most vulnerable tracheids of the stem, not a pore that will be seen frequently in SEM views. The largest visible pores in figure 5*E* are about 1.5 times smaller, on the order of 0.1 μm. Similarly, *Zygogynum pancherii*'s cavitation threshold of −4.5 MPa corresponds to a pore of ca. 0.07 μm, which is about 1.4 times the size of the largest 0.05-μm pores in the membrane in figure 5*D*.

The complications of pit membrane heterogeneity are not unique to vesselless angiosperms. Exceptionally large holes have been observed in a subsample of intervessel/intervasicentric tracheid pit membranes in some vessel-bearing angiosperms (Sano 2005; Sano and Jansen 2006) and perhaps are responsible in part for the considerable variation in average pit resistances measured in eudicots (range: 39–2035 MPa s m^{-1}; Hacke et al. 2006). Interestingly, these holes are also generally confined to the periphery of the pit membrane, as observed for *T. aralioides* and *P. traversii* (fig. 5*A*, 5*B*). These observations raise the possibility of "cryptic" vessels even in vessel-bearing taxa.

The apparently derived position of Winteraceae and Trochodendrales in the angiosperm phylogenetic tree means that either they reverted to the vesselless condition or that vessels evolved independently in several more basal lineages (Young 1981; Baas and Wheeler 1996; Doyle 2000; Carlquist and Schneider 2002; Feild et al. 2002). Our results do not decide between these alternatives, but they do not yield any obvious signal of a reversion to vessellessness. In nearly all ways, the tracheids of the derived vesselless taxa functioned in a similar manner as those of the ancestrally vesselless *A. trichopoda*. The only exception was greater permeability to the silicone/Uvitex injection in *A. trichopoda* tracheids, suggesting a more sustained longitudinal alignment of permeable pit membranes. Nevertheless, *A. trichopoda* had a relatively high pit area resistance ($r_P = 23 \pm 6$ MPa s m^{-1}) in association with its relatively large tracheids. High pit area resistance suggests that exceptionally large membrane holes were rare, consistent with none being observed in the SEM. Perhaps this is indicative of poorly developed perforations in its cyptic vessels, a very speculative observation but one consistent with a basal position for the species.

Two other species that stand out, not for having exceptional silicone penetration but in a different parameter, are *T. aralioides* and *T. sinense*. All other species had extremely similar fractions of their tracheid wall area occupied by pits (F_P; table 1), averaging 0.064 ± 0.002. In contrast, the fraction in these two species was more than twice as high (0.16 ± 0.009 in *T. sinense*, 0.18 ± 0.07 in *T. aralioides*; table 1). Although this trait is seemingly uninformative with respect to a potentially vesseled ancestry, it was consistent with *T. aralioides* being relatively vulnerable to cavitation despite its rather small tracheid size ($D = 12.4 \pm 0.3$ μm). According to the pit area hypothesis, a large pit area will confer greater vulnerability even if it is contained in a small tracheid. It is also consistent with *T. sinense*'s being the most vulnerable of all vesselless species because of the combination of high pitting percentage, large tracheids ($D = 21.4 \pm 0.8$ μm), and low-resistance pit membranes with reportedly large pores (Carlquist 1992*a*).

Although the vesselless angiosperms were more efficient as a group than we expected, clearly eudicot vessels are still superior (fig. 9). However, all of the eudicot species in that data set had simple perforation plates and represent the most derived of vessel morphology (Hacke et al. 2006). In a companion article (Sperry et al. 2007), we compare our results for vesselless angiosperms with results from some of their close vessel-bearing relatives, many of which have rather "primitive" vessel morphologies (Bailey 1953; Carlquist 1992*a*). In this way, we can infer how the transition from tracheids to vessels influenced conducting efficiency and vulnerability to cavitation.

Acknowledgments

The work was funded by National Science Foundation grant IBN-0416297 to J. S. Sperry. The University of Utah granted J. S. Sperry full sabbatical leave to collect material for the project. Sherwin Carlquist advised him at early stages on localities and taxon sampling. On-site experts aided collection and identification: Stuart Worboys, Tony Bean, Barbara Rice (Australia), Gordon McPherson (New Caledonia), Phil Knightbridge (New Zealand), Takefumi Ikeda (Japan), Armando Soto and Barry Hammel (Costa Rica), Francesco Squeo (Chile), and Holly Forbes (Berkeley Botanical Garden). Fred Adler (University of Utah) suggested the use of the Weibull function for improving the accuracy of deriving tracheid-length distributions from silicone injections. Y. Sano was supported by a Grant-in-Aid for Scientific Research (18580158) from the Ministry of Education, Culture, Sports, Science, and Technology, Japan.

Literature Cited

Alder NN, WT Pockman, JS Sperry, S Nuismer 1997 Use of centrifugal force in the study of xylem cavitation. J Exp Bot 48:665–674.

Andre JP 2005 Vascular organization of angiosperms: a new vision. Science, Enfield, NH. 154 pp.

Baas P, EA Wheeler 1996 Parallelism and reversibility in xylem evolution: a review. IAWA J 17:351–364.

Bailey IW 1953 Evolution of the tracheary tissue of land plants. Am J Bot 40:4–8.

Carlquist S 1975 Ecological strategies of xylem evolution. University of California Press, Berkeley. 259 pp.

——— 1983 Wood anatomy of *Bubbia* (Winteraceae), with comments on origin of vessels in dicotyledons. Am J Bot 70:578–590.

——— 1987 Presence of vessels in wood of *Sarcandra* (Chloranthaceae): comments on vessel origins in angiosperms. Am J Bot 74: 1765–1771.

——— 1988 Wood anatomy of *Drimys sensu stricto* (Winteraceae). Aliso 12:81–96.

——— 1990 Wood anatomy of *Ascarina* (Chloranthaceae) and the tracheid-vessel element transition. Aliso 12:667–684.
——— 1992*a* Pit membrane remnants in perforation plates of primitive dicotyledons and their significance. Am J Bot 79:660–672.
——— 1992*b* Wood anatomy of *Hedyosmum* (Chloranthaceae) and the tracheid-vessel element transition. Aliso 13:447–462.
Carlquist S, EL Schneider 2002 The tracheid-vessel transition in angiosperms involves multiple independent features: cladistic consequences. Am J Bot 89:185–195.
Choat B, EC Lahr, PJ Melcher, MA Zwieniecki, NM Holbrook 2005 The spatial pattern of air-seeding thresholds in mature sugar maple trees. Plant Cell Environ 28:1082–1089.
Cohen S, JP Bennink, MT Tyree 2003 Air method measurements of apple vessel length distributions with improved apparatus and theory. J Exp Bot 54:1889–1897.
Doyle JA 2000 Paleobotany, relationships, and geographic history of Winteraceae. Ann Mo Bot Gard 87:303–316.
Feild TS, NC Arens 2005 Form, function and environments of the early angiosperms: merging extant phylogeny and ecophysiology with fossils. New Phytol 166:383–408.
Feild TS, T Brodribb, NM Holbrook 2002 Hardly a relict: freezing and the evolution of vesselless wood in Winteraceae. Evolution 56: 464–478.
Feild TS, NM Holbrook 2000 Xylem sap flow and stem hydraulics of the vesselless angiosperm *Drimys granadensis* (Winteraceae) in a Costa Rican elfin forest. Plant Cell Environ 23:1067–1077.
Feild TS, MA Zwieniecki, TJ Brodribb, T Jaffre, MJ Donoghue, NM Holbrook 2000 Structure and function of tracheary elements in *Amborella trichopoda*. Int J Plant Sci 161:705–712.
Hacke UG, JS Sperry, J Pittermann 2005 Efficiency vs. safety trade-offs for water conduction in angiosperm vessels vs. gymnosperm tracheids. Pages 333–353 *in* NM Holbrook, M Zwieniecki, eds. Vascular transport in plants. Elsevier Academic, Amsterdam.
Hacke UG, JS Sperry, WP Pockman, SD Davis, KA McCulloh 2001 Trends in wood density and structure are linked to prevention of xylem implosion by negative pressure. Oecologia 126:457–461.
Hacke UG, JS Sperry, JK Wheeler, L Castro 2006 Scaling of angiosperm xylem structure with safety and efficiency. Tree Physiol 26:689–701.
Hargrave KR, KJ Kolb, FW Ewers, SD Davis 1994 Conduit diameter and drought-induced embolism in *Salvia mellifera* Greene (Labiatae). New Phytol 126:695–705.
Lancashire JR, AR Ennos 2002 Modelling the hydrodynamic resistance of bordered pits. J Exp Bot 53:1485–1493.
Niklas KJ 1994 Plant allometry. University of Chicago Press, Chicago. 395 pp.
Pittermann J, JS Sperry, UG Hacke, JK Wheeler, EH Sikkema 2005 Torus-margo pits help conifers compete with angiosperms. Science 310:1924.
——— 2006*a* Inter-tracheid pitting and the hydraulic efficiency of conifer wood: the role of tracheid allometry and cavitation protection. Am J Bot 93:1105–1113.
Pittermann J, JS Sperry, JK Wheeler, UG Hacke, EH Sikkema 2006*b* Mechanical reinforcement of tracheids compromises the hydraulic efficiency of conifer xylem. Plant Cell Environ 29:1618–1628.
Pockman WT, JS Sperry 2000 Vulnerability to cavitation and the distribution of Sonoran desert vegetation. Am J Bot 87:1287–1299.
Sano Y 2005 Inter- and intraspecific structural variation among intervascular pit membranes, as revealed by field-emission scanning electron microscopy. Am J Bot 92:1077–1084.
Sano Y, S Jansen 2006 Perforated pit membranes in imperforate tracheary elements of some angiosperms. Ann Bot 97:1045–1053.
Soltis PS, DE Soltis 2004 The origin and early diversification of angiosperms. Am J Bot 91:1614–1626.
Sparks JP, RA Black 1999 Regulation of water loss in populations of *Populus trichocarpa*: the role of stomatal control in preventing xylem cavitation. Tree Physiol 19:453–459.
Sperry JS, UG Hacke, TS Feild, Y Sano, EH Sikkema 2007 Hydraulic consequences of vessel evolution in angiosperms. Int J Plant Sci 168: 1127–1139.
Sperry JS, UG Hacke, J Pittermann 2006 Size and function in conifer tracheids and angiosperm vessels. Am J Bot 93:1490–1500.
Tyree M, S Davis, H Cochard 1994 Biophysical perspectives of xylem evolution—is there a tradeoff of hydraulic efficiency for vulnerability to dysfunction? IAWA J 15:335–360.
Wheeler JK, JS Sperry, UG Hacke, N Hoang 2005 Inter-vessel pitting and cavitation in woody Rosaceae and other vesselled plants: a basis for a safety vs. efficiency trade-off in xylem transport. Plant Cell Environ 28:800–812.
Young DA 1981 Are the angiosperms primitively vesselless? Syst Bot 6:313–330.
Zimmermann MH 1983 Xylem structure and the ascent of sap. Springer, Berlin. 143 pp.
Zimmermann MH, AA Jeje 1981 Vessel length distribution of some American woody plants. Can J Bot 59:1882–1892.
Zwieniecki MA, PJ Melcher, NM Holbrook 2001 Hydrogel control of xylem hydraulic resistance in plants. Science 291:1059–1062.